Communications in Nonlinear Science and Numerical Simulation 114 (2022) 106683

Contents lists available at ScienceDirect

Communications in Nonlinear Science and Numerical Simulation

journal homepage: www.elsevier.com/locate/cnsns

Research paper

Enhanced complexity of chaos in micro/nanoelectromechanical beam resonators under two-frequency excitation

André Gusso [a,*], Ricardo L. Viana [b], Sebastian Ujevic [a]

[a] Departamento de Ciências Exatas-EEIMVR, Universidade Federal Fluminense, Volta Redonda, RJ, 27255-125, Brazil
[b] Departamento de Física, Universidade Federal do Paraná, Curitiba, PR 81531-980, Brazil

ARTICLE INFO

Article history:
Received 18 March 2021
Received in revised form 6 May 2022
Accepted 22 June 2022
Available online 26 June 2022

Keywords:
Nonlinear dynamics
Chaos
Robust chaos
Microelectromechanical systems
Nanoelectromechanical systems

ABSTRACT

Suspended beam micro/nanoelectromechanical (MEMS/NEMS) resonators are relevant potential sources of chaotic signals for many practical applications due to their low power consumption and high operating frequencies. However, chaos is generally restricted to small regions of the parameter space when MEMS/NEMS resonators are driven by a single frequency, as considered so far in most of the literature and all experiments. It has recently been found that strong chaotification and robust chaos (characterized by a chaotic attractor insensitive to changes on the system parameters) can emerge in the resonators when excited by two distinct frequencies. Here we show that this strong chaotification not only increases the regions in the parameter space with chaos, but also enhances the complexity of the chaotic dynamics. These findings make MEMS/NEMS resonators even more attractive for practical applications. The increase in complexity is demonstrated through the analysis of the Fourier spectrum and the use of recurrence quantification analysis (RQA). A larger entropy of the Fourier spectrum and lower determinism are obtained compared to the single frequency excitation as the amplitude of the second frequency increases.

1. Introduction

Suspended beam micro and nanoelectromechanical (MEMS/NEMS) have been widely investigated, both theoretically and experimentally [1,2], due to their many potential applications. They can be used as high quality factor filters for electronic signals, ultrastable reference clocks and a variety of physical and chemical sensors, that rely upon their operation in a linear regime [1,2]. More recently, some strategies to take advantage of the nonlinear behavior have been proposed to improve signal amplification [3] and frequency stability [4], among other applications [5]. The existence of chaos in suspended beam resonators was predicted theoretically in several works [6–11]. It was verified experimentally for two coupled nanomechanical beam resonators [12] and, more importantly, also for a suspended beam MEMS resonator of the kind considered in this work [13]. As it was already proposed for other configurations of MEMS/NEMS resonators [14], suspended beam resonators have the potential to be used as sources of chaotic signals for applications in chaos based secure communications, cryptography and random number generation [15–17]. Because of their smallness, high frequency

* Corresponding author.
E-mail address: andregusso@id.uff.br (A. Gusso).

https://doi.org/10.1016/j.cnsns.2022.106683
1007-5704/

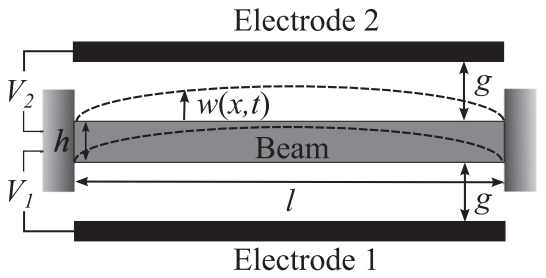

Fig. 1. Schematic diagram of the doubly clamped suspended beam resonator (gray) with two lateral electrodes (black).

of vibration and low power consumption, suspended beam MEMS/NEMS resonators are ideal candidates as a physical source of continuous chaotic signal or entropy in mobile devices.

In spite of their many interesting advantages, MEMS/NEMS resonators when operated in its most usual setups quite generally present weak chaos. This form of chaos is characterized as having a chaotic attractor that is destroyed by small changes of the system parameters leading the system to oscillate periodically or move into another chaotic attractor with distinct dynamics. Furthermore, it was shown in Ref. [7] that for beam resonators actuated by only one lateral electrode, chaos was obtained on a tiny region of the relevant parameter space. In the case of beams actuated by two electrodes, it was shown in Ref. [18] that when only one electrode is used to drive the beam with an AC voltage, chaos also occur only in comparatively small and disconnected regions in the $V_{AC} - V_{DC}$ plane. Such circumstances can prevent or make it very difficult to take advantage of the chaotic regime of suspended beam MEMS/NEMS resonators. One way to circumvent such limitations is the use of two-frequency (2f) excitation [19]. When each electrode of a two-electrode resonator is excited with an AC voltage with different frequencies a much larger region in the parameter space presents chaos. Furthermore, it was shown in Ref. [19] that the chaos is robust in a significant portion of the relevant parameter space. Robust chaos is characterized by the persistence of the chaotic attractor with changes of the system parameters [16,20], and it is generally required for practical applications of chaotic systems. Therefore, 2f-excitation leads not only to a desirable increase in the availability of chaos in the system, but also the chaotic attractor has essentially the same dynamical and statistical properties under small changes, or fluctuations, in the system parameters. After the numerical evidences presented in Ref. [19] the use of 2f-excitation has attracted increased attention. This is evidenced by the recent experimental investigations of the chaotification induced by 2f-excitation in MEMS described as single-well Duffing oscillators. The experiments were performed with a doubly clamped suspended microbeam [21] and a MEMS drum resonator [22]. While chaos was observed where it was not expected in the case of single frequency excitation, in both experiments the regions with chaos were mixed with regions of regular dynamics, indicating that the attractor was not robust. This result for the case of systems with a dynamics dictated by the equation of a single-well Duffing oscillator could be expected from the numerical analysis presented in Ref. [23].

The fact that a two-electrode beam resonator can now present robust chaos makes this system a strong candidate for practical applications as a source of a continuous time chaotic signal. This is important since only a couple of other continuous time dynamical systems with robust chaos, such as the Lorenz equations, have been mentioned in the literature and could be available for practical applications. It was also recently demonstrated that the Duffing oscillator under 2f-excitation also presents strong chaotification and robust chaos [23]. However, as the chaotification induced by 2f-excitation has only recently been identified in theoretical works [19], it requires further investigation. For this reason, in this work we investigate theoretically the periodic and chaotic regimes of the doubly-clamped two electrode suspended beam resonator excited by two frequencies, depicted schematically in Fig. 1. We compare the dynamics obtained with the usual single-frequency (1f) excitation with that with 2f-excitation. We first study how the regions with chaos in phase diagrams (or state diagrams) change as the amplitude of a second AC voltage is changed. We then characterize how the initially periodic or chaotic dynamics evolves as the amplitude of the second AC voltage is increased, with a focus on the resulting complexity of the chaos. The entropy of the Fourier spectrum and measures from recurrence quantification analysis (RQA) are used to characterize the complexity of the dynamics. The analysis of the complexity of the chaotic dynamics as a function of the applied voltages is motivated by the fact that many applications can benefit from an enhanced complexity of chaotic dynamics. That is the case of broad band telecommunications and chaos based radars, which rely upon signals with a broad Fourier spectrum [20,24].

The work is organized as follows. In Section 2 we present the physical and mathematical model of the MEMS/NEMS resonator. The chaotification is investigated using phase diagrams in Section 3, showing the regions with periodicity, chaos and pull-in, in the relevant parameter space, as function of the amplitude of the second applied voltage. In Section 4 the entropy of the Fourier spectrum is analyzed and used to investigate how the complexity of the chaotic dynamics changes as the second frequency increases in amplitude. In Section 5 RQA is used with the same purpose of investigating the complexity of chaos. In Section 6 we consider the changes on the basins of attraction and the role of the initial conditions on the results of the previous sections. We conclude in Section 7.

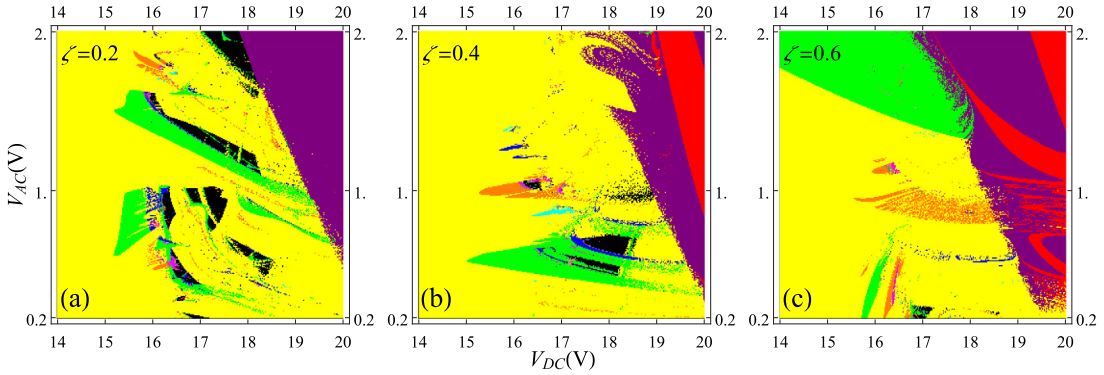

Fig. 2. Phase diagrams in the $V_{AC}-V_{DC}$ plane obtained for a single excitation frequency and $\beta = 0.01$. Results for normalized frequencies $\zeta = 0.2$, 0.4, and 0.6. The diagrams show the regions with periodic, chaotic and pull-in attractors. The color code is the following. For the periodic attractors: yellow → period $T = 2\pi/\zeta$, green → 2T, orange → 3T, blue → 4T, cyan → 5T, magenta → 6T, white → 7T, brown → 8T. Periods above 9T are colored gray. The pull-in to the electrode located at $s = -1(s = 1)$ is colored red(purple), and chaos is presented in black.

2. Physical and mathematical model

The physical and mathematical model we use to describe the system depicted in Fig. 1, is well known in the literature [9,18,19,25], and it is only briefly reviewed in this section.

The device we are going to investigate is comprised of a slender beam with length l and with a rectangular cross section of width b and thickness h. The beam is clamped at both ends and there are electrodes parallel to its width placed a distance g at both sides of the beam. This arrangement is depicted schematically in Fig. 1. The beam is considered to have homogeneous and isotropic elastic properties. Because in the strong nonlinear regime that we investigate here the beam can be subject to large transversal displacements we have to include the effect of the midplane stretching [25]. It is responsible for a nonlinear hardening effect of the elastic restoring force. The beam is actuated by electrostatic forces due to the voltages V_1 and V_2 applied between the electrodes and the beam. In the modeling of the electrostatic force we consider the beam to be piecewise plane and ignore the fringing effect, because the beams are wide, minimizing this effect. Linear viscous damping is assumed as the only form of energy dissipation. Nonlinear damping may also exist in suspended beam micro and nanoresonators, as already evidenced experimentally [26]. However, we do not include nonlinear damping in the physical model because the proposed nonlinear damping mechanisms, like those in Refs. [27,28], have only been studied in the weak nonlinear (quasilinear) regime and the theoretical results cannot be extended to model nonlinear damping in a chaotic regime. The inclusion of such effects in the simulation of the chaotic dynamics is an interesting theoretical challenge.

Within the proposed model the transverse beam displacement $w(x, t)$ has to satisfy the following partial differential equation [9]

$$\rho A\ddot{w} + c\dot{w} + EIw'''' - \left(\frac{EA}{2l}\int_0^l w'^2 dx\right) w'' = \frac{\epsilon_0 b}{2}\left[\frac{V_2(t)^2}{(g-w)^2} - \frac{V_1(t)^2}{(g+w)^2}\right]. \tag{1}$$

In this equation the primes represent derivatives with respect to space x while the overdots derivatives with respect to time t, ρ denotes the density and E the material's Young modulus. The beam is assumed to have a rectangular cross-section with a geometric moment of inertia $I = bh^3/12$, and cross-sectional area $A = bh$. The linear damping coefficient is c and $\epsilon_0 = 8.85 \times 10^{-12}$ F/m corresponds to the vacuum permittivity.

The equation is reduced to a single nonlinear ordinary differential equation (NLODE) using the Galerkin method [25]. We consider that the beam vibrates at frequencies below or about its first resonance frequency and use a single mode approximation taking $w(x, t) = q(t)\phi_1(x)$, where $\phi_1(x)$ denotes the base function which corresponds to the first modeshape of a doubly clamped beam described mathematically by the Euler–Bernoulli beam equation [25].

The resulting equation is

$$\ddot{s} + \beta\dot{s} + s + \alpha s^3 + F^e(s, \tau) = 0\,. \tag{2}$$

In this NLODE $s = s(\tau)$ is the nondimensional displacement of the beam center. More specifically, $s(\tau) = q(\tau)w_{max}/g$, where $w_{max} = w(x = 0.5l, \tau)$ corresponds to the maximum beam displacement that occurs at $x = 0.5l$. Time t is replaced by the nondimensional time $\tau = t/\omega_1$, where ω_1 denotes the natural frequency of the first mode. The strength of the cubic nonlinearity is $\alpha = 0.719(g/h)^2$, and the damping factor β can be shown to be related to the quality factor Q simply by $\beta = Q^{-1}$.

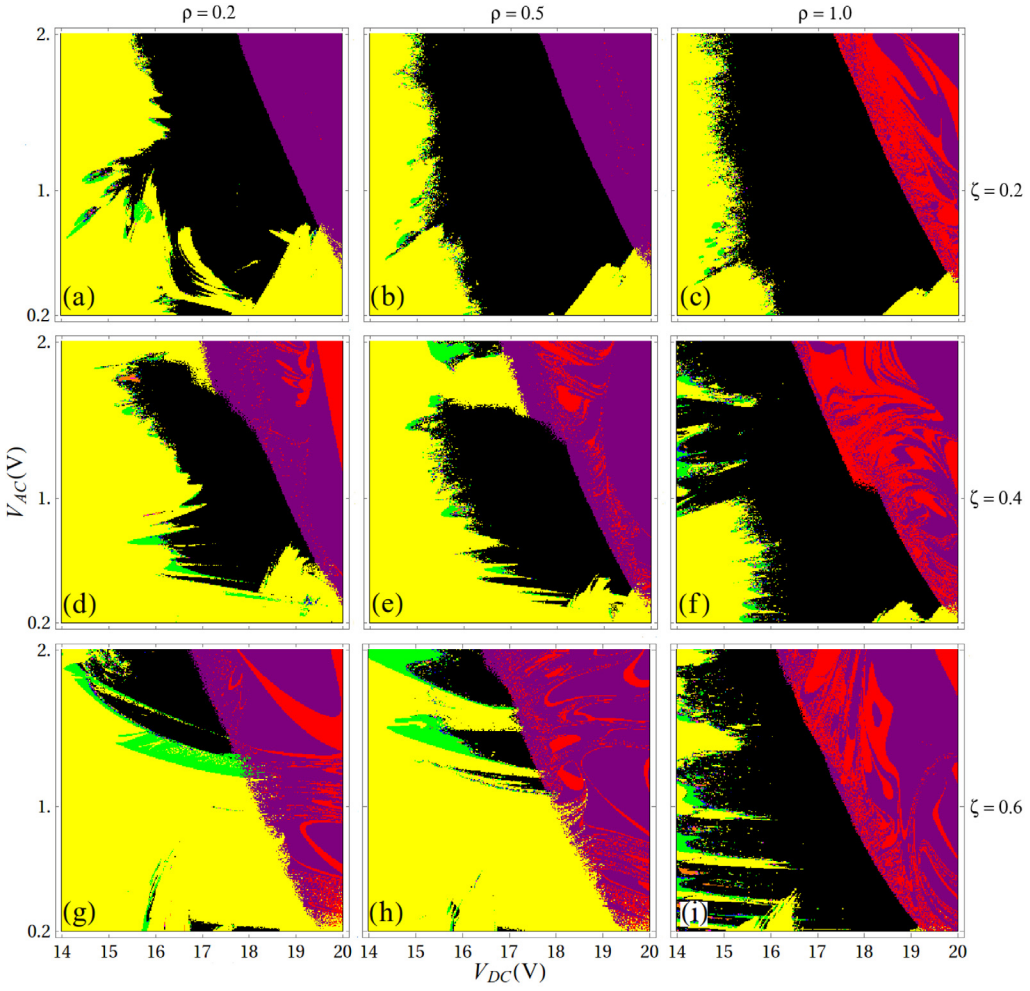

Fig. 3. Phase diagrams in the $V_{AC} - V_{DC}$ plane obtained for two excitation frequencies with $\beta = 0.01$ and frequency ratio $r = 1.07$. From the top to the bottom line of figures the frequencies are $\zeta = 0.2, 0.4$, and 0.6, respectively. In figures (a), (d) and (g) $V_{AC,2} = \rho V_{AC,1}$ with $\rho = 0.2$, in (b), (e) and (h) $\rho = 0.5$, and in (c), (f) and (i) $\rho = 1$. The diagrams show the regions with periodic, chaotic and pull-in attractors. The color code is the same as that in Fig. 2, but with $T = 107 \times 2\pi/\zeta$.

The last term in Eq. (2) corresponds to the effective electrostatic force, and is given by

$$F^e(s,\tau) = 1.218\frac{\epsilon_0 bl}{2k_{eff}d^3}\left[V_1^2(\tau)\int_0^1 \frac{\phi_1(x')}{(1+\phi_1(x')s/g)^2}dx' - V_2^2(\tau)\int_0^1 \frac{\phi_1(x')}{(1-\phi_1(x')s/g)^2}dx'\right]$$
$$= B\left[V_1^2(\tau)I^e(s) - V_2^2(\tau)I^e(-s)\right], \tag{3}$$

where $B = 0.609\epsilon_0 bl/(k_{eff}d^3)$, $k_{eff} = 384EI/l^3$ denotes the effective elastic constant of the beam, the new variable x' is the normalized length position $x' = x/l$, and $I^e(s)$ is representing the integral that is a function of s.

Eq. (2) is an integro-differential equation, whose direct numerical solution is computationally quite demanding because it involves to solve two integrals numerically. In order to solve this NLODE in an efficient manner, we follow the procedure adopted in Refs. [7,9,18,19] and replace the integrals $I^e(s)$ in $F^e(s,\tau)$ by a suitable approximate function in the form of a Padé approximant

$$I_a^e(s) = \frac{a_0 + a_1 s}{(1 + \sum_{i=1}^{3} b_i s^i)}. \tag{4}$$

The coefficients a_i and b_i are obtained using the least squares fit so that $I_a^e(s)$ is close enough to the value of $I^e(s)$ obtained by numerical integration within a suitable interval in the variable s. As we have observed that the system oscillates with amplitudes not exceeding $|s| \sim 0.7$, in this work the coefficients have been calculated to ensure a precise result for $I_a^e(s)$ in the range $-0.8 \leq s \leq 0.8$. Using the Padé approximant of order 1/3 in Eq. (4) it is possible to obtain a maximum error of

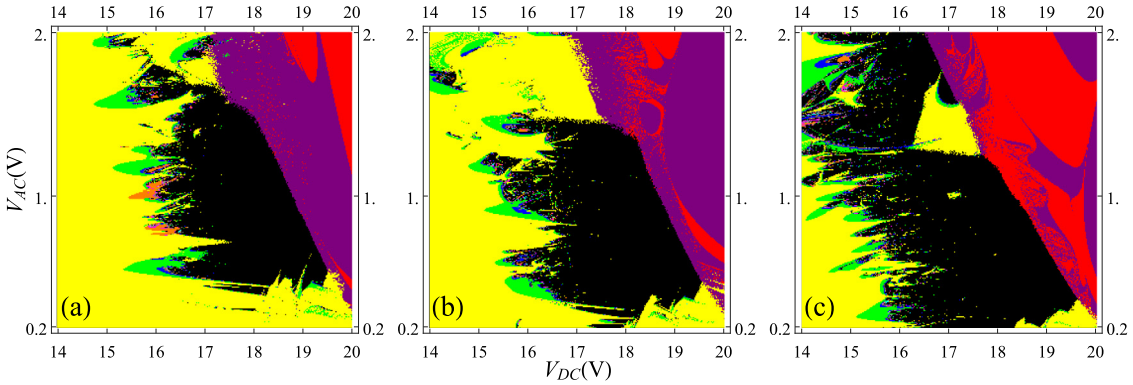

Fig. 4. Figures (a), (b) and (c) represent the same cases depicted in Figs. 3(d), (e), and (f), respectively, but for $r = 1.3$.

about 0.1% in the approximation to the function $I^e(s)$ within this interval. The approximation is still quite reliable outside the above interval, and is used to identify when the system has suffered pull-in (the beam is attracted and gets attached to one of the electrodes due to the electrostatic force caused by the applied DC voltage bias, V_{DC}). In the numerical solution we have taken into account that the results cannot be outside the interval $|s| < 1$, because the electrodes are located at $s = \pm 1$, and if s comes sufficiently close to the electrodes the system will fatally stop to oscillate due to the dynamical pull-in. In practice, we stop the numerical calculations when $|s|$ exceeds a certain value, which we take to be $|s| = 0.95$.

In the great majority of the works investigating the nonlinear dynamics and chaos of resonators with a configuration similar to the one considered here the system is excited by a single frequency [8,9,18]. In these cases the excitation is performed by applying voltages of the form $V_1(\tau) = V_{DC} + V_{AC,1}\cos(\zeta\tau)$ and $V_2(\tau) = V_{DC}$ at each lateral electrode. The DC voltage V_{DC} is introduced to change the effective potential of the system [8]. For sufficiently large V_{DC} applied to both electrodes a double-well potential develops, which favors the appearance of chaos. In this work an additional AC voltage with a different frequency is applied and we have $V_2(\tau) = V_{DC} + V_{AC,2}\cos(\zeta\tau/r)$, where $r > 1$ denotes the frequency ratio. As pointed in Ref. [19] the addition of this second AC excitation greatly enhances the generation of chaos on the system. However, the investigation was limited to the case in which both AC voltages have the same magnitude, and the focus was to demonstrate that there was a region in the relevant parameter space in which chaos was robust. The investigation of the robustness of chaos was limited to a subregion because a much more detailed and time consuming numerical analysis was required. In the next sections new results and analysis are presented for the case of 2f-excitation of a nanoresonator.

3. Chaotification

In this section we investigate how the initially very small regions with chaos in the parameter space evolves into a much larger and continuous region with chaos. In this and the next sections we present results for a nanoresonator whose dimensions are $l = 5$ μm, $b = 0.8$ μm and $h = 0.05$ μm. The gap is chosen based upon a criteria that facilitates the appearance of a double-well potential [8,9], which favors a chaotic dynamics, and is taken to be $d = 0.15$ μm. The device is considered to be made of polysilicon, whose Young modulus is $E = 170$ GPa and the density $\rho = 2.3 \times 10^3$ kg m^{-3} [25]. With these dimensions and materials, the predicted natural frequency of the first mode is $f = 17.7$ MHz, in the absence of any applied voltage. We assume $\beta = 0.01$ throughout the work. This value of the damping parameter was shown in Ref. [19] to be small enough for the system to develop robust chaos. Larger values, above approximately 0.03, results in a significant decrease of the regions with chaos. If damping is also too small ($b \lesssim 0.001$) multistability becomes prevalent and the continuous regions with chaos tend to disappear. In this and in the next two sections, the numerical solutions of Eq. (2) are all obtained for the same initial conditions (ICs) $s(0) = v(0) = 0$, where $v = \dot{s}$. The role of the ICs in our results and conclusions is discussed in Section 6.

For later comparison we present in Fig. 2 the phase diagrams in the $V_{AC} - V_{DC}$ plane obtained when the AC voltage is applied only in electrode 1, that means $V_{AC,2} = 0$, which is analogous to that in Ref. [18]. Note that in this case the regions in the parameter space where chaos is observed are small and disconnected islands in a sea of periodic dynamics. In this case the periodic motion can occur with periods that are integer multiples of the period of the excitation frequency ($T_1 = 2\pi/\zeta$).

Let us now introduce the second AC voltage, $V_{AC,2}$. Its effect is to increase the regions with chaos, which also become more connected as $V_{AC,2}$ increases. This is shown in Fig. 3 for representative values of frequency ($\zeta = 0.2$, 0.4, and 0.6). A large and continuous region with chaos is observed even for $V_{AC,2}$ as small as $0.2V_{AC,1}$ the region being larger for lower frequencies. As ζ increases the region with chaos shrinks. For $\zeta = 0.6$ this region is not only significantly smaller, but also contains tongues of periodic dynamics that penetrate deep into it. Therefore, chaos is favored by smaller ζ. It can

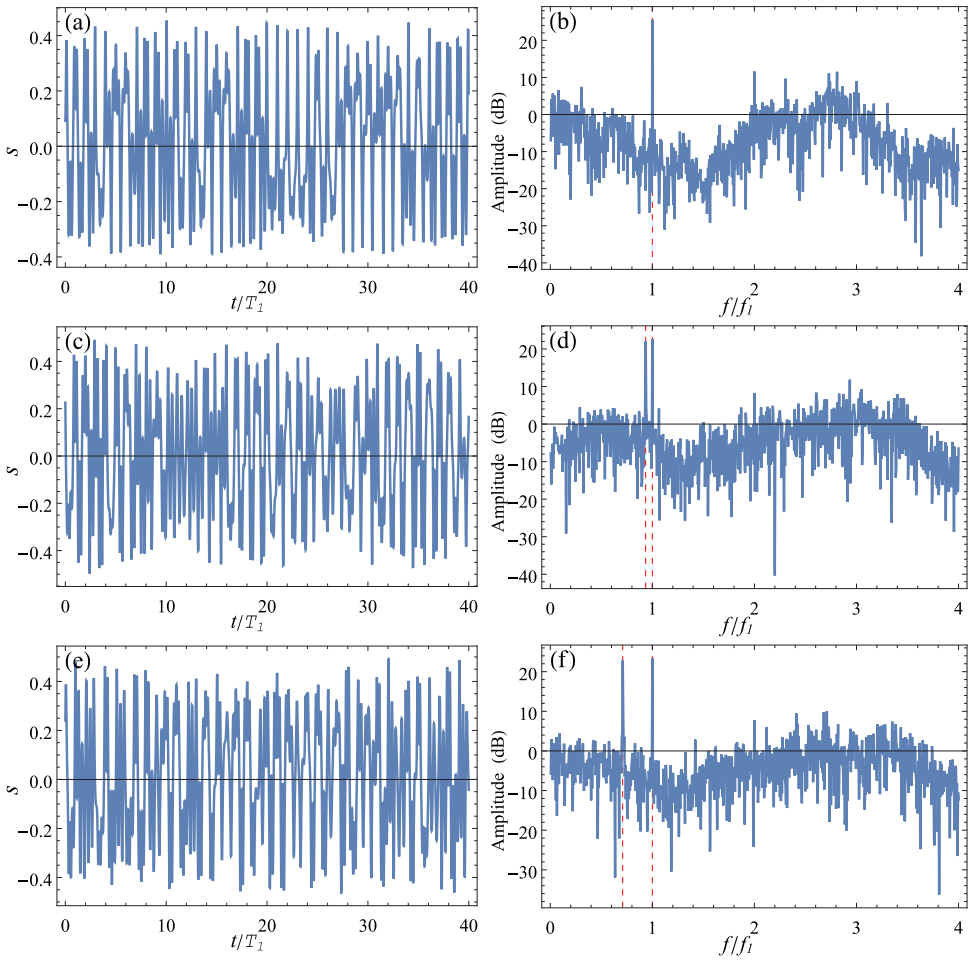

Fig. 5. Displacement $s(t)$ and power spectrum for chaotic dynamics obtained with 1f ((a) and (b)) and 2f-excitation with $r = 1.07$ ((c) and (d)) and $r = 1.41$ ((e) and (f)). Results obtained for $\zeta = 0.2$, $V_{AC} = 0.9$ V and $V_{DC} = 17.4$ V. Time and frequency are normalized by $T_1 = 2\pi/\zeta$ and $f_1 = T_1^{-1}$. The red vertical lines indicate the frequencies of excitation. For small values of r, such as $r = 1.07$, we observe in the chaotic dynamics a slow frequency envelope. This phenomenon occurs due to the frequency beat, as the two excitations are superimposed. This may be an undesirable feature in a chaotic signal in practical applications. Fortunately, this problem can be eliminated by the use of larger r. For instance, the oscillations in the time domain for $r = 1.41$ (a rational number close to $\sqrt{2}$) show no evidence of an envelope, and similar results are obtained when $r \gtrsim 1.2$.

also be seen in Fig. 3 that the periodic region for 2f-excitation presents a simpler topology when compared with the 1f-frequency case. This region is dominated by period-one oscillations and comparatively smaller regions with period-two. Very few areas in the periodic region have signs of multistability (intermingled attractors) which are much more common for a single frequency of excitation. Before we proceed, we have to point that when the resonator is excited by two frequencies it does not synchronize with either periods $T_1 = 2\pi/\zeta$ or $T_2 = 2\pi r/\zeta$. Instead, if the frequency ratio r is a rational number of the form $r = n/m$, $n, m \in N^*$, the lowest possible periodic motion has period $T = nT_1 = mT_2$. If r is irrational, only quasi-periodic motion can be expected. Since the results in Fig. 3 are for $r = 1.07$ a period-one oscillation corresponds to a period $T = 107 \times T_1$, where T_1 is the period of the period-one oscillations seen in Fig. 2.

One of the findings in Ref. [19] was that the regions with robust chaos could degrade significantly for specific frequency ratios that can be given as the ratio of small natural numbers. This conclusion was reached through the calculation of the fraction of periodic points within the region in the parameter space where robust chaos was sought. However, no detailed investigation on how this change happened within this region was performed. For this reason we have generated phase diagrams for the frequencies for which the regions with chaos seemed to degrade. The results are illustrated in Fig. 4 for $r = 1.3$ and $\zeta = 0.4$. For this r the period doubling cascades towards chaos are more evident. More importantly, tongues of periodic behavior penetrate in the region of chaos and small periodic regions spread all over it. In this scenario it may be impossible to warrant that the resonator starts and remains in a chaotic regime during operation. Fortunately, for practical applications of chaos, for essentially any other rational frequency ratio we have tested, the phase diagrams are similar to those in Fig. 3.

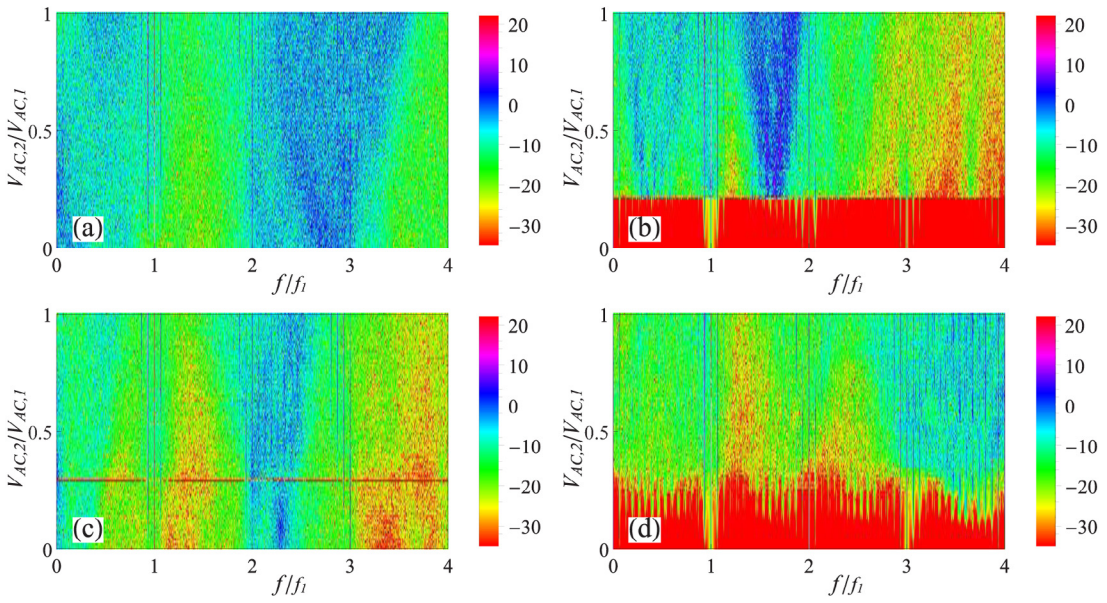

Fig. 6. Power spectrum obtained with 2f excitation as a function of the voltage ratio $\rho = V_{AC,2}/V_{AC,1}$. Frequencies are normalized by $f_1 = 1/T_1 = \zeta/2\pi$. In all cases $r = 1.07$ and (a) $\zeta = 0.2$, $V_{AC} = 0.9$ V, and $V_{DC} = 17.4$ V, in (b) $\zeta = 0.4$, $V_{AC} = 1.0$ V, and $V_{DC} = 16.7$ V, in (c) $\zeta = 0.2$, $V_{AC} = 0.5$ V, and $V_{DC} = 16.5$ V, and in (d) $\zeta = 0.2$, $V_{AC} = 1.8$ V, and $V_{DC} = 15.4$ V. The colors indicate the amplitude of the components of the spectrum in dB.

4. Spectral entropy

The usefulness of a dynamical system for practical applications, such as a source of chaotic signal, depends not only on the reliable existence of the desired dynamical state, but also on its characteristics on the time and frequency domains. In Section 3 we have seen how the regions with periodicity and chaos change for different values of the ratio $\rho = V_{AC,2}/V_{AC,1}$. The best results, regarding the chaotification, are obtained for $\rho = 1$. However, we do not know how the chaotic dynamics is changing as we vary ρ. The characterization of the chaotic dynamics is important as it may determine the usefulness of the obtained chaos for a particular application. For instance, the use in radars and broadband communication requires a large and flat Fourier spectrum [29]. For applications such as random number generation, unpredictability or randomness, are the desired features [30].

For this reason we perform a more detailed analysis of the dynamics of the resonator under 2f-excitation. We have varied the amplitude of the second applied frequency, from zero up to a voltage equal to that applied in the first electrode. What we have found is that the chaotic dynamics becomes evidently more complex in time and frequency domains with the introduction of a second frequency. This is illustrated in Fig. 5, where results for 1f and 2f-excitation are compared. The increase in complexity seen in the time domain for the 2f-excitation will be accessed in the next section using RQA. In this section we analyze the richer frequency spectrum obtained with the 2f-excitation, which in the case illustrated in Fig. 5 has stronger contributions at frequencies both above and below the driving frequencies compared to the 1f-excitation.

The analysis of the Fourier spectrum has the advantage of providing us simultaneously with information regarding its broadband nature and the complexity of the dynamics. It is generally accepted that a broader(narrower) spectrum reflects a more(less) complex chaotic dynamics. We have investigated how the Fourier spectrum changes as ρ increases from 0 up to 1 to see how the spectrum and complexity are influenced by the second frequency. The spectra can be analyzed qualitatively through the visualization of the periodograms. Four representative periodograms are presented in Fig. 6. Panels (a) and (c) correspond to points within one of the chaotic islands in Fig. 2(a) when $\rho = 0$. The difference observed in (c) is that a tiny periodic window appears at $\rho = 0.29$. There were other cases of points in the parameter space having chaos when $\rho = 0$ that presented a regular behavior over small windows in the parameter ρ. However, the windows generally appear for $\rho \lesssim 0.5$. This indicates that it is safer to produce chaos using ρ close to or equal to one, thus avoiding that uncontrollable changes in the system parameters lead it to operate within a periodic window. Panels (b) and (d) in Fig. 6 correspond to points with periodic dynamics when $\rho = 0$. As ρ increases chaos emerges in both cases. In (b) a sudden transition to chaos is visible in the spectrum, and it was checked that it also appears in the corresponding bifurcation diagram at $\rho = 0.216$. This result suggests crisis as the underlying mechanism for the generation of chaos. Crisis is by far the most frequent mechanism by which chaos emerges or disappears as ρ varies. While in Fig. 6(d) there seems to be a smooth transition to chaos the bifurcation diagrams have shown that regularity and chaos are intermingled in a transition region that starts at $\rho = 0.30$ and extends approximately up to $\rho = 0.35$. While suggestive of intermittency [31] further investigation of this region has not evidenced the intermittency between

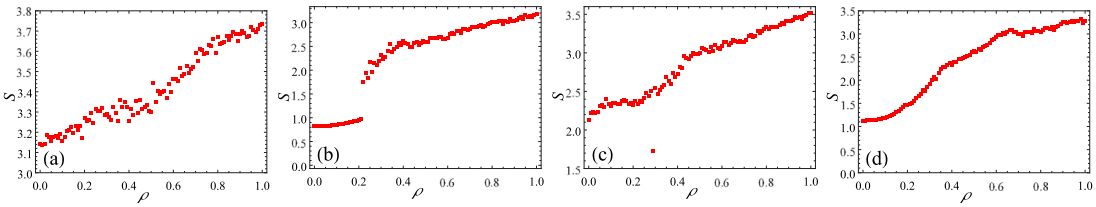

Fig. 7. Spectral entropy S as a function of the voltage ratio ρ for the corresponding periodograms in Fig. 6.

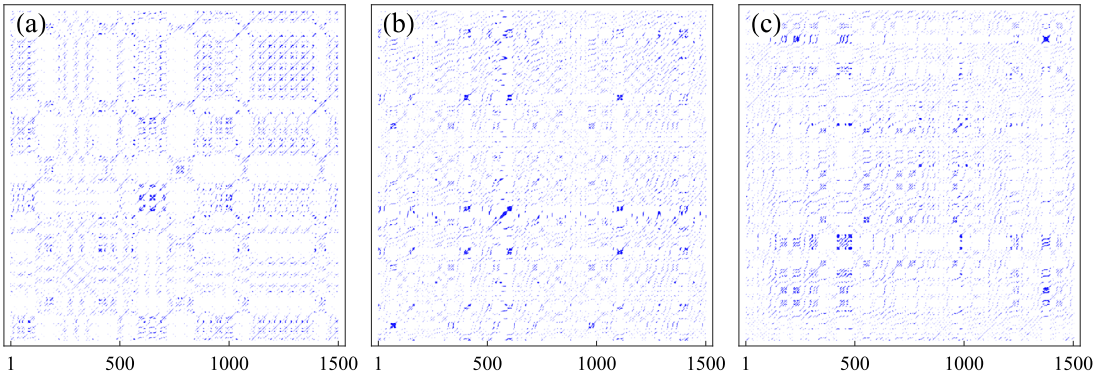

Fig. 8. Recurrence plots of the dynamics of nanoresonator excited with $\zeta = 0.2$, $V_{AC,1} = 0.9$ V, and $V_{DC} = 17.4$ V and (a) $V_{AC,2} = 0$ V, (b) $V_{AC,2} = 0.9$ V and $r = 1.07$, and (c) $V_{AC,2} = 0.9$ V and $r = 1.41$. The RPs span a total time of $30 \times T_1$ ($T_1 = 2\pi/\zeta$), with recurrence times t_i ($i = 0, \ldots, 1500$) at intervals equal to $T_1/50$. All RPs have been obtained for constant recurrence ratio $RR = 3\%$.

chaotic and periodic attractors over the time evolution of the system. Less frequently the bifurcation mechanism is also observed. We note, however, that despite its relevance the main focus of this work is not the study of the mechanism leading to chaos but, instead, its complexity.

In Fig. 6 all the spectra present a larger dispersion of frequencies as ρ increases (seen as an increase in green and blue areas). This trend was also observed in all other periodograms we have analyzed. While the visual inspection of the periodograms supports this conclusion, to characterize more precisely the changes of the Fourier spectrum we resorted to a more quantitative analysis. The dispersion of the spectrum was quantified by means of its spectral entropy (SE) [32]. The SE is defined in terms of the normalized amplitudes of the Fourier spectrum,

$$p_i = \frac{|a_i|^2}{\sum_i |a_i|^2}\,, \tag{5}$$

where the a_i are the complex spectral amplitudes, and the sum is performed over all frequencies considered in the spectrogram. The spectral entropy is then

$$S = -\sum_i p_i \ln p_i\,. \tag{6}$$

As the details of the Fourier spectrum depends upon the time window over which the time series of $s(t)$ is sampled, in what follows we show results for S calculated as the average over four SEs calculated at different times. We take four consecutive time windows with length $\Delta t = 200T_1$ ($T_1 = 2\pi/\zeta$) starting after a transient time equal to $3000T_1$. Other sets of time windows have also been considered and the results obtained where essentially the same. The SE was calculated considering frequencies f in the range $0 \le f/f_1 \le 4$, where $f_1 = 1/T_1$ is the largest of the two excitation frequencies.

In Fig. 7 it is shown the SE corresponding to the spectra in Fig. 6. In Figs. 7(a) and (c) the systems is always in a chaotic state, except for the point of regularity seen in (c). In (b) the sudden change to chaos ($\rho = 0.216$) is reflected in the SE, and in (d) the SE changes smoothly and the regularity/chaos transition that starts at $\rho = 0.30$ cannot be identified. For our purpose, which is the investigation of the complexity of the chaotic dynamics, the most important feature of the SE is that it increases with ρ when the system is in a region with chaos, the largest SE being always obtained for $\rho = 1$. While we present results for $r = 1.07$, the results are quite analogous for other r we have investigated.

5. Recurrence quantification analysis

While the SE is a good measure for the complexity of chaos there are other quantifiers that can be used to address this complexity as well. RQA is a comparatively simple method of analysis that provide us with some relevant measures

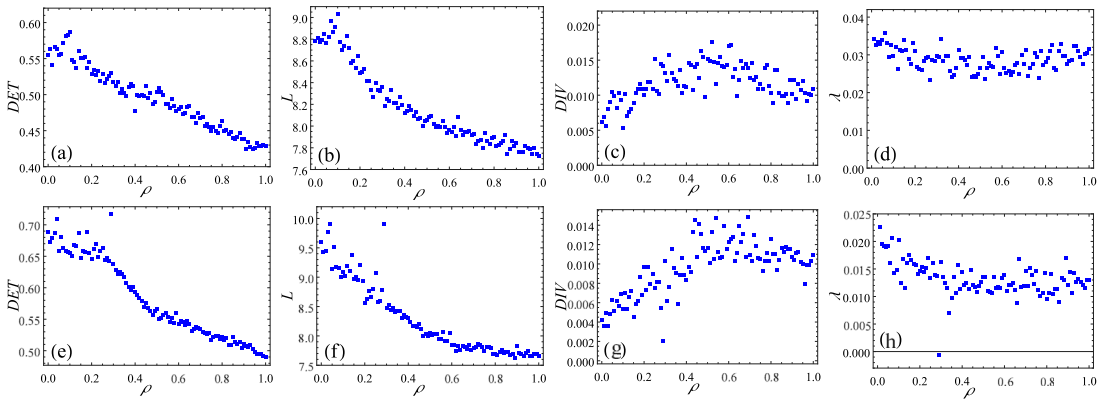

Fig. 9. RQA measures *DET*, *L* and *DIV* and the maximum Lyapunov exponent λ as a function of ρ. (a),(b),(c), and (d) have parameters $r = 1.07$, $\zeta = 0.2$, $V_{AC} = 0.9$ V, and $V_{DC} = 17.4$ V, while for (e), (f), (g), and (h) $r = 1.07$, $\zeta = 0.2$, $V_{AC} = 0.5$ V, and $V_{DC} = 16.5$ V.

of complexity [33]. RQA is based on the quantitative analysis of recurrence plots (RPs). A RP shows how often the neighborhood of a given point in the phase space of a dynamical system is visited by the trajectory at later times. It is obtained in the form of a $N \times N$ matrix, with elements $R(i, j)$ assuming the value 1 when in the time t_j the trajectory comes sufficiently close to where it was in the time t_i, $i, j \in \{t_0, t_1, t_2, \ldots, t_N\}$, being zero otherwise. Periodic trajectories in the phase space result in parallel straight diagonal lines in RPs, while a uncorrelated stochastic trajectory results in a random distribution of points. Chaotic trajectories results in complex structures, their complexity varying quite significantly between different dynamical systems. In Fig. 8 we present representative RPs obtained for the nanoresonator. These RPs were obtained considering the same frequency and voltages used to generate Fig. 6(a). In Fig. 8(a), (b) and (c) we can identify complex patterns commonly obtained for chaotic systems, mixing regular structures and disordered regions. In the RP obtained for 1f-excitation, Fig. 8(a), we can see more regular structures than for the other two RPs, Figs. 8(b) and (c), obtained for 2f-excitation and differing only in the frequency ratio r. Therefore, these RPs suggest that 2f-excitation leads to a more complex, unpredictable dynamics.

While visual inspection of RPs can be useful to draw qualitative conclusions about the dynamics of a system, quantitative results are obtained using RQA. The complexity of the chaotic dynamics is reflected in several RQA quantifiers like the determinism (*DET*), average length of diagonals (*L*), and the inverse of the maximum length of the diagonals (*DIV*) (see, for instance, Ref. [33], for the detailed definition of these quantifiers). *DET* varies between 0 and 1, and measures how deterministic a time series is. Lower values of DET are an indication of less predictable or uncorrelated dynamics. It takes on smaller values for stochastic processes, but is not zero since spurious recurrences by pure chance can occur even in strongly noisy series. Therefore, small values of *DET* reflect a more complex, less predictable, chaotic dynamics. *L* brings information which is similar to that of *DET*. Smaller *L* indicates a less predictable dynamics. *DIV* is related to the exponential divergence of the phase space trajectory. The faster the trajectory segments diverge, the shorter are the diagonal lines and the higher is the measure *DIV* [33]. Therefore, a large *DIV* is expected to reflect a more stochastic dynamics.

We have investigated numerically how these quantifiers change with ρ using the commandline recurrence plots (RPs) program made available by Marwan [34]. The RPs have been calculated for fixed values of the recurrence ratio (*RR*) using a routine which adapted the values of radius of neighborhood (ϵ), so as to make comparisons more reliable. Different values of *RR* varying between 1% and 5% have been tested and no significant qualitative changes have been observed in this range. In what follows we present results for an intermediary value $RR = 2.5\%$. The minimum diagonal and vertical line lengths have also been varied between 2 and 10. For lengths above 3 or 4 the results where found to be always in good qualitative agreement, and the results presented here are for a minimum length of 5. The stability with changes in both *RR* and minimum line lengths indicates that our conclusions drawn from the analysis of the RPs are reliable for any *RR* and lengths taken within the above mentioned intervals. As in the determination of the spectral entropy *S*, we have considered four distinct time intervals after the transient of $3000T_1$ to perform the RQA. Four time intervals with length $50T_1$ have been sampled with frequency $T_1/50$ resulting in a data series for the recurrence plots with a length of 2500 points. The presented results are the average over the four estimates for the RQA quantifiers.

In Fig. 9 we show *DET*, *L* and *DIV* as a function of ρ for two illustrative cases. Both *DET* and *L* tend to decrease as ρ increases towards one. The same trend was observed for all other sets of parameters ζ, V_{AC} and V_{DC} we have investigated. In the case of *DIV* it tends to increase when *DET* and *L* decrease significantly. When the two other measures suffer small increases *DIV* may either increase for small values of ρ later reaching a plateau for large ρ or reach a fuzzy maximum for ρ around 0.5 later decreasing slightly for larger ρ.

It is important to note that both *DET* and *L* have shown a strong dependence on ρ. In the cases presented in Fig. 9 *L* decreases by as much as 20% while *DET* by 30%, and frequently larger changes have been observed for other cases we have

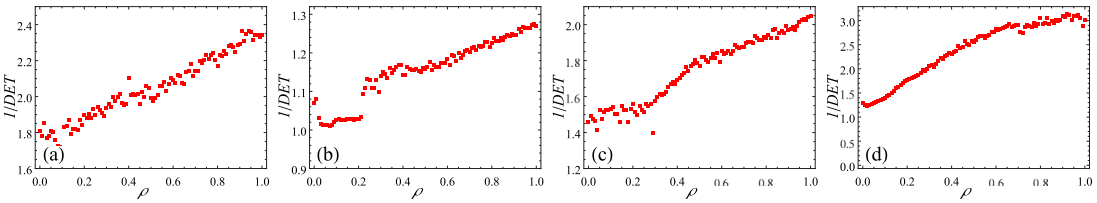

Fig. 10. Results for $1/DET$ corresponding to the same four set of parameters in Fig. 7 showing the striking similarity between the two measures of the complexity of chaos.

investigated. These consistent and large changes indicate that setting a constant *RR* is allowing to interpret the obtained results as a reliable indication of changes in the complexity of the chaotic dynamics.

Therefore, two out of the three main RQA indicators of complexity of the chaotic dynamics corroborate the conclusion obtained from the entropy of the Fourier spectrum. And while *DIV* does not fully agree with the other measures it is not in strong contradiction. We have also calculated the maximum Lyapunov exponent λ as a function of ρ. What we observed is that it is generally weak correlated with the changes in the spectrum and of the RQA parameters. While a positive Lyapunov exponent is a predictor of chaos it alone cannot fully characterize the properties of a chaotic attractor [35].

Further comparison of the spectral entropy and the RQA measures indicates that *S* and *DET* are anticorrelated, as expected, one increasing where the other decreases and vice-versa. And while *L* is also anticorrelated with *S*, a stronger connection between *S* and *DET* was observed. The investigation of this anticorrelation led us to conclude that for the system we have studied the quantity $1/DET$ is strongly correlated with *S*, presenting an strikingly similar dependence on ρ. This can be seen from the comparison of the results for *S* in Fig. 7 with those for $1/DET$ obtained for the same four sets of parameters and presented in Fig. 10. Therefore, our results indicate that $1/DET$ could be used as a measure of the spectral entropy, and vice-versa. Investigating further this connection between $1/DET$ and *S* in beyond the scope of this work, however, it deserves further numerical and theoretical investigation, including other dynamical systems.

6. Basins of attraction under 2f-excitation

So far, our results have been obtained assuming always the same IC, $s(0) = v(0) = 0$. However, the phase diagrams presented in Fig. 2 for the case of 1f-excitation present regions with signs of multistability, where different attractors are intermingled in a very intricate, seemingly random patterns. The presence of such regions in the phase diagrams are, in general, an indication of the sensitivity of the system to the ICs within these regions. This fact was confirmed by the analysis in Ref. [18], in which complex intermingled or fractal basins of attraction have been found for points in these regions of the phase diagrams.

We have to note that, in its turn, there is little evidence of multistability in the phase diagrams obtained for 2f-excitation in Fig. 3. Only the region of the frontier between regular and chaotic motion have a small transition region where attractors seem to be mixed. The exception is the case of excitation with the higher frequency $\zeta = 0.6$, where a frontier with more signs of multistability is observed. Therefore, based upon the phase diagrams we can conclude that the 2f-excitation has the effect of reducing the multistability observed for 1f-excitation. It leads to more well defined regions of periodicity, chaos and pull-in, particularly for smaller excitation frequencies.

However, in order to properly access the question of the multistability the basins of attraction must be investigated. Such an analysis was already performed for the case of 1f-excitation by two of the authors in Ref. [18], considering the same system and the parameter space we investigate in this work. While basins with a single periodic or chaotic attractor were the most commonly found basins in this case, mixed and fractal basins were also frequently observed within the region defined in Fig. 2.

In the case of 2f-excitation, what we concluded is that the presence of the second voltage leads quite generally to more robust basins. That means, there is a single prevailing region in the $s - v$ space of ICs with a single attractor, either periodic or chaotic. While few cases of basins with more than one attractor are observed for $\rho \lesssim 0.5$, for larger values of ρ no multistable basins have been found within the regions where the chaotification occurs.

These findings are illustrated by the basins of attraction calculated for different ρ for the parameters corresponding to those of Figs. 6(b) and (c), which are presented in Fig. 11. First, let us note that the basins are formed by an inner region containing periodic, chaotic or mixed attractors, surrounded by two other regions colored purple and red, that corresponds to pull-in to the electrodes at $s = 1$ or $s = -1$, respectively. We are not interested in the basins that lead to pull-in, and the corresponding ICs must be avoided in practical applications. However, due to the presence of thermal noise or small environmental vibrations, the ICs may differ slightly from $s(0) = v(0) = 0$ when the driving voltages are turned on. With regard to the relevant inner region, it is interesting to see that for $\rho = 0$ Figs. 11(a) and (f) have basins with two distinct attractors. However, when $\rho = 0.2$ the basins present a single attractor, and as ρ is further increased the single attractor becomes chaotic for both cases. This trend was also observed in the basins calculated using the parameters of Figs. 6(a) and (d). While not shown, the basins for $\rho = 1$ have been calculated and are quite similar to those for $\rho = 0.8$.

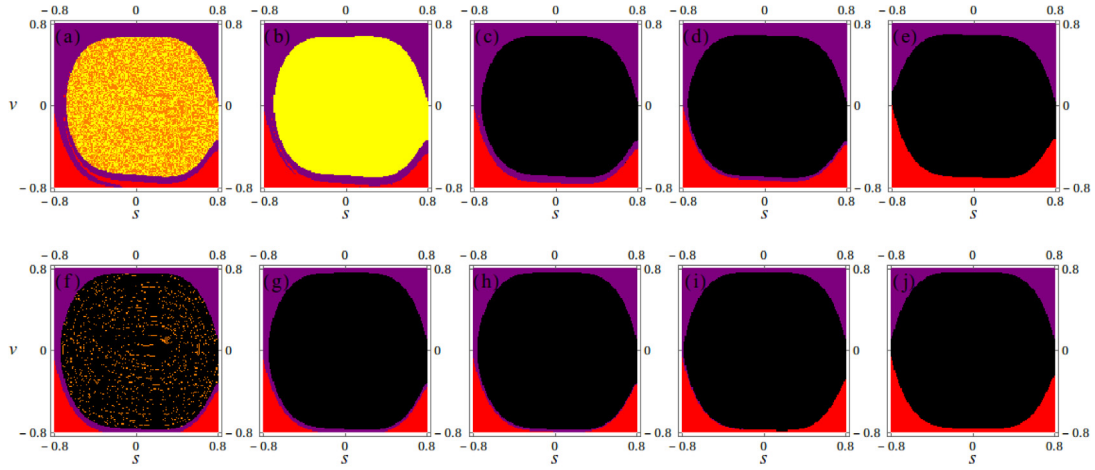

Fig. 11. The figures in the upper and lower lines depict the basins of attraction obtained for the same parameters as those for Fig. 6(b) and (c), respectively. From left to right $\rho = 0, 0.2, 0.4, 0.6$, and 0.8. The color code is the same as that defined in Fig. 2.

This behavior of the basins is important, since it assures the robustness of the chaotic attractor obtained with 2f-excitation for sufficiently large ρ [19]. It is also important because our main results and conclusions about the increase of the complexity of the chaotic dynamics with ρ become independent of the ICs. To illustrate that, in Fig. 12 we show the spectral entropy obtained for varying ICs for the corresponding cases in Figs. 7(b) and (c). For most values of ρ the resulting S differs only due to statistical fluctuations, which result from the limited sampling of the chaotic attractor. However, for a few points satisfying $\rho \lesssim 0.5$ different results are obtained for different ICs due to the presence of more than one attractor in the basin. The presence of two attractors in the inner region of the basins seen for $\rho = 0$ in Fig. 11(a) is reflected as two distinct values of S. The lower entropy is obtained for period T oscillations, while the larger entropy, with a values close to that observed in the chaotic regimes, corresponds to period $3T$ oscillations. However, for the basin in Fig. 11(f) we do not see two significantly different values of S, because the vibrations with period $3T$ have such a complexity that the entropy is almost as high as that for the chaotic regime under 1f-excitation ($\rho = 0$), as already observed in Fig. 12(a). In Fig. 12(b) for two values of ρ between 0.2 and 0.3 the entropy S changes significantly due to the existence of basins with mixed periodic and chaotic attractors. To conclude, we have to mention that, while not shown for the sake of clarity in the figures, we have considered as much as 100 different random ICs in the calculation of S, the results being essentially the same as those presented in Fig. 12. We have also performed the same calculations with 100 ICs for the other two cases presented in Fig. 7, and no significant departures from what was presented were observed.

7. Discussion and conclusions

Chaos was recently obtained experimentally in a MEMS resonator with a configuration analogous to the one we have been considering in our theoretical analysis [13] using 1f-excitation, as well as, on other MEMS using 2f-excitation [21,22]. These result highlights the potential of such systems as sources of chaotic signals for practical applications. Motivated by its technological relevance, in this work we have further investigated the nonlinear and chaotic dynamics of a suspended beam bridge resonator actuated with two distinct AC signals through its two lateral electrodes. We have shown how the dynamics evolves from one dominated by periodic attractors to one with a large and continuous region with chaos in the $V_{AC} - V_{DC}$ plane. It was also seen how the periodic and chaotic dynamics for 2f-excitation differs from that with 1f-excitation. In particular, we have seen that the chaotic dynamics has a broader frequency spectrum, which may be useful for practical applications, such as broadband communication or radars [29].

The spectral entropy, DET and L indicate consistently that the chaotic dynamics is more complex in the presence of the second applied voltage. In general, values of $V_{AC,2}$ comparable to those of $V_{AC,1}$ lead to the more complex dynamics. Certain applications can benefit from this complexity. That is the case, for instance, of the generation of random numbers, which was investigated in Ref. [30] considering as the source of entropy the device studied in this work.

To conclude, we have shown in this work that the 2f-excitation not only induces robust chaos over small regions of the parameter space, as demonstrated in Ref. [19], it also results in a quite significant increase of the region in the parameter space where chaos, robust or not, can be expected. We have also concluded that the chaotic dynamics is generally more complex for larger values of the second applied voltage. Therefore, the 2f-excitation, comes with two important, and for certain applications beneficial, consequences for the chaotic dynamics of micro and nanoresonators of the kind we have investigated.

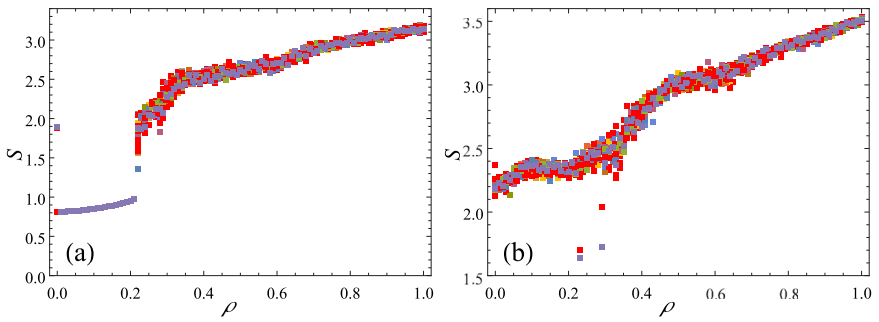

Fig. 12. Spectral entropy S calculated for 20 different ICs. (a) and (b) were obtained for the same parameters as those for Fig. 6(b) and (c), respectively. The ICs were varied randomly within the region $-0.4 \leq s, v \leq 0.4$. Colors are used to distinguish the results for the distinct ICs.

CRediT authorship contribution statement

André Gusso: Conceptualization, Methodology, Formal analysis, Software, Writing – original draft. **Ricardo L. Viana:** Conceptualization, Methodology, Writing – review & editing. **Sebastian Ujevic:** Conceptualization, Methodology, Software, Writing – original draft.

Declaration of competing interest

The authors declare that they have no known competing financial interests or personal relationships that could have appeared to influence the work reported in this paper.

Acknowledgments

A. Gusso is thankful to W. G. Dantas for helpful discussions on the applications for random number generation. R. L. Viana was supported by CNPq-Brasil.

References

[1] Huang XMH, Feng XL, Zorman CA, Mehregany M, Roukes ML. VHF UHF and microwave frequency nanomechanical resonators. New J Phys 2005;7:247.
[2] Uranga A, Verd J, Barniol N. CMOS-MEMS resonators: from devices to applications. Microelectron Eng 2015;132:58–73.
[3] Almog R, Zaitsev S, Shtempluck O, Buks E. Signal amplification in a nanomechanical duffing resonator via stochastic resonance. Appl Phys Lett 2007;90:013508.
[4] Antonio D, Zanette DH, López D. Frequency stabilization in nonlinear micromechanical oscillators. Nature Commun 2012;3:806.
[5] Rhoads J, Shaw SW, Turner KL. Nonlinear dynamics and its applications in micro- and nanoresonators. J Dyn Sys Meas Control 2010;132:034001.
[6] Alemansour H, Miandoab EM, Pishkenari HN. Effect of size on the chaotic behavior of nano resonators. Commun Nonlinear Sci Numer Simul 2017;44:495–505.
[7] Amorim TD, Dantas WG, Gusso A. Analysis of the chaotic regime of MEMS/NEMS fixed–fixed beam resonators using an improved 1DOF model. Nonlinear Dynam 2015;79:967–81.
[8] Barceló J, Rosselló JL, Bota S, Segura J, Verd J. Electrostatically actuated microbeam resonators as chaotic signal generators: a practical perspective. Commun Nonlinear Sci Numer Simul 2016;30:316–27.
[9] Dantas WG, Gusso A. Analysis of the chaotic dynamics of MEMS/NEMS doubly clamped beam resonators with two–sided electrodes. Int J Bifurc Chaos 2018;28:1850122.
[10] De SK, Aluru NR. Complex oscillations and chaos in electrostatic microelectromechanical systems under superharmonic excitations. Phys Rev Lett 2005;94:204101.
[11] Haghighi HS, Markazi AHD. Chaos prediction and control in MEMS resonators. Commun Nonlinear Sci Numer Simul 2010;15:3091–9.
[12] Karabalin RB, Cross MC, Roukes ML. Nonlinear dynamics and chaos in two coupled nanomechanical resonators. Phys Rev B 2009;79:165309.
[13] Barceló J, de Paúl I, Bota S, Segura J, Verd J. Chaotic signal generation in the MHz range with a monolithic CMOS-mems microbeam resonator. In: Proc. 2019 IEEE int. conf. microeletromech. syst.. 2019, p. 1037–40.
[14] Wang YC, Adams SG, Thorp JS, MacDonald NC, Hartwell P, Bertsch F. Chaos in MEMS, parameter estimation and its potential application. IEEE Trans Circuits Syst I 1998;45:1013–20.
[15] Cuomo KM, Oppenheim AV. Circuit implementation of synchronized chaos with applications to communications. Phys Rev Lett 1993;71:65–8.
[16] Kocarev L. Chaos-based cryptography: a brief overview. IEEE Circuits Syst Mag 2001;1:6.
[17] Verschaffelta G, Khoder M, Van der Sande G. Random number generator based on an integrated laser with on-chip optical feedback. Chaos 2017;27:114310.
[18] Gusso A, Viana RL, Mathias AC, Caldas IL. Nonlinear dynamics and chaos in micro/nanoelectromechanical beam resonators actuated by two-sided electrodes. Chaos Soliton Frac 2019;122:6–16.
[19] Gusso A, Dantas WG, Ujevic S. Prediction of robust chaos in micro and nanoresonators under two-frequency excitation. Chaos 2019;29:033112.
[20] Zeraoulia E, Sprott JC. Robust chaos and its applications. Singapore: World Scientific Publishing; 2012.
[21] Houri S, Asano M, Yamaguchi H, Yoshimura N, Koike Y, Minati L. Generic rotating-frame-based approach to chaos generation in nonlinear micro- and nanoelectromechanical system resonators. Phys Rev Lett 2020;125:174301.

[22] Defoort M, Rufer L, Fesquet L, Basrour S. A dynamical approach to generate chaos in a micromechanical resonator. Microsyst Nanoeng 2021;7:17.
[23] Gusso A, Ujevic S, Viana RL. Strong chaotification and robust chaos in the duffing oscillator induced by two-frequency excitation. Nonlinear Dynam 2021;103:1955–67.
[24] Carroll TL. Optimizing chaos-based signals for complex radar targets. Chaos 2007;17:033103.
[25] Younis MI. MEMS Linear and nonlinear statics and dynamics. New York: Springer; 2011.
[26] Zaitsev S, Shtempluck O, Buks E, Gottlieb O. Nonlinear damping in a micromechanical oscillator. Nonlinear Dynam 2012;67:859–83.
[27] Gusso A. Nonlinear damping in doubly clamped beam resonators due to the attachment loss induced by the geometric nonlinearity. J Sound Vib 2016;372:255–65.
[28] Gusso A. Nonlinear damping in suspended beam micro- and nanoresonators due to surface loss. J Sound Vib 2020;467:115067.
[29] Leung H. Chaotic signal processing. Philadelphia: SIAM; 2013.
[30] Dantas WG, Rodrigues LR, Ujevic S, Gusso A. Using nanoresonators with robust chaos as hardware random number generators. Chaos 2020;30:043126.
[31] Manffra EF, Caldas IL, Viana RL, Kalinowski HJ. Type-i intermittency and crisis–induced intermittency in a semiconductor laser under injection current modulation. Nonlinear Dynam 2002;27:185–95.
[32] Powell GE, Percival IC. A spectral entropy method for distinguishing regular and irregular motion of Hamiltonian systems. Phys A Math Gen 1979;12:2053–71.
[33] Marwan N, Romano MC, Thiel M, Kurths J. Recurrence plots for the analysis of complex systems. Phys Rep 2007;438:237–329.
[34] Marwan N. Calculations of the RQA measures were performed using the software commandline RP. 2006, available at https://tocsy.pik-potsdam.de.
[35] Farmer D, Crutchfield J, Froehling H, Packard N, Shaw R. Power spectra and mixing properties of strange attractors. Ann NY Acad Sci 1980;357:453–71.